C. Casty · D. Handorf · C. C. Raible
J. F. González-Rouco · A. Weisheimer · E. Xoplaki
J. Luterbacher · K. Dethloff · H. Wanner

Recurrent climate winter regimes in reconstructed and modelled 500 hPa geopotential height fields over the North Atlantic/European sector 1659–1990

Abstract Recurrent climate winter regimes are examined from statistically reconstructed and modelled 500 hPa geopotential height fields over the North Atlantic/ European sector for the period 1659–1990. We investigate the probability density function of the state space spanned by the first two empirical orthogonal functions of combined winter data. Regimes are detected as patterns that correspond to areas of the state space with an unexpected high recurrence probability using a Monte Carlo approach. The reconstruction and the model reveal four recurrent climate regimes. They correspond to the two phases of the North Atlantic Oscillation and two opposite blocking patterns. Complemented by the investigation of the temporal evolution of the climate regimes this leads to the conclusion that the reconstructed and the modelled data for this geographic sector reproduce low-frequency atmospheric variability in the form of regime-like behaviour. The overall evidence for recurrent climate regimes is higher for the model than for the reconstruction. However, comparisons with independent data sources for the period 1659–1990 revealed a more realistic temporal evolution of the regimes for the reconstructed data.

C. Casty · E. Xoplaki · J. Luterbacher · H. Wanner
Institute of Geography, University of Bern,
Hallerstrasse 12, 3012 Bern, Switzerland

C. Casty (✉) · E. Xoplaki · J. Luterbacher · H. Wanner
NCCR Climate, University of Bern, Switzerland
E-mail: casty@giub.unibe.ch
Tel.: +41-31-6318545
Fax: +41-31-6318511

D. Handorf · K. Dethloff
Alfred Wegener Institute for Polar and Marine Research,
Potsdam, Germany

C. C. Raible
Climate and Environmental Physics, University of Bern,
Switzerland

J. F. González-Rouco
Department of Astrophysics and Atmospheric Sciences,
University of Madrid, Spain

A. Weisheimer
Institute of Meteorology, Free
University of Berlin, Germany

1 Introduction

Starting from the early work of Rossby (1939), many studies revealed that atmospheric variability is characterised by a few preferred recurrent and/or persisting large-scale flow patterns, which occur at fixed geographical regions. Therefore, the concept of atmospheric circulation regimes has been developed to connect these observations with atmospheric dynamics. In general, flow patterns that persist longer than the typical and synoptical time scale of about 10 days are defined as weather regimes and detected on the basis of daily data. Preferred flow patterns determined on the basis of monthly mean data are generally referred to as climate regimes. In the framework of the concept of climate regimes, low-frequency climate variability can arise due to transitions between the distinct atmospheric regimes and is manifested, primarily, in terms of changes in the frequency of occurrence of the preferred circulation regimes (Palmer 1999). If the concept of regimes is proven, a better understanding of long-term variability and the improvement of long-range forecasts of the climate system behaviour by identifying those regimes can be achieved.

Several methods have been developed for the detection of weather and climate regimes. Baur et al. (1944) introduced a phenomenological approach with the concept of the so-called "Grosswetterlagen". In this approach, the classification of daily weather maps is based on the assumption that only a finite number of

atmospheric states exists. A more advanced concept is the search for teleconnected regions in atmospheric data, incipient by investigating correlation maps (e.g. Exner 1924; Walker 1924; Wallace and Gutzler 1981), to the nowadays commonly used method of principal component or EOF-analysis (e.g. Barnston and Livezey 1987). To prove the existence of multiple weather/climate regimes, more advanced methods are applied today. This includes cluster analysis (e.g. Mo and Ghil 1988; Cassou et al. 2004), the detection of local density maxima in the reduced state space of atmospheric data (e.g. Molteni et al. 1988; Kimoto and Ghil 1993a, 1993b; Corti et al. 1999), the search for quasi-stationary states in the reduced state space (e.g. Hannachi 1997), or extended versions of principal component analysis (e.g. Vautard 1990; Monahan et al. 2001). The studies analysing observed atmospheric data give evidence for the existence of multiple (two to six) weather/climate regimes for the Northern Hemisphere. A summarising table of these studies regarding their data basis and number of identified regimes is given in Stephenson et al. (2004).

Moreover, several climate models have confirmed the regime behaviour of the northern hemispheric flow. The analysis of different model runs (e.g. Hannachi 1997; Hsu and Zwiers 2001; Raible et al. 2001; Weisheimer et al. 2001) mostly revealed regimes which are known from observational analysis. Furthermore, studies of model runs with increased greenhouse gases show a general tendency towards a decreased number of preferred regimes, but no change of their spatial structure (e.g. Monahan et al. 2000).

Accepting the existence of weather/climate regimes, the question arises regarding the underlying dynamical processes. The fundamental paper by Charney and DeVore (1979) was the first to explain atmospheric flow regimes as multiple equilibria, thus associated with stable fixed points of the state space. In subsequent studies with low-order nonlinear dynamical systems, multiple regimes were related to metastable fixed points or other simple attracting invariant sets (e.g. Lorenz 1963; De Swart 1988; Legras and Ghil 1985; Palmer 1993, 1999). Hasselmann (1999) proposed an explanation for multiple regimes even in high-dimensional systems taking the model of a stochastically forced particle moving around several potential wells.

External forcing influences the frequency of occurrence of preferred circulation regimes. Palmer (1999) suggested a dynamical paradigm for climate change. Accordingly, a (weak) external forcing does not change the spatial pattern, but results in frequency changes of occurrence of the weather/climate regimes. This dynamical paradigm is supported by e.g. Corti et al. (1999) on the basis of the northern hemispheric 500 hPa geopotential height fields.

Based on the above-mentioned studies, we consider the concept of weather/climate regimes caused by the nonlinear dynamics of the atmosphere as useful for understanding low-frequency variability in observational data and simulations with complex climate mod-els. The studies of Hsu and Zwiers (2001), Yang and Reinhold (1991) and Stephenson et al. (2004) stated that observational time series are too short to identify recurrent climate regimes and their changes with statistical significance and that such analyses should be performed on a sectoral basis. A possibility to fulfil these requirements is the use of reconstructions of past climate periods.

We aim at investigating the evidence for climate regimes in a 330-year long data set of reconstructed 500 hPa geopotential height fields (Luterbacher et al. 2002) for the North Atlantic/European sector. Till now, this data set has been unique and very useful for comparison with the simulated regime variability in complex climate models. Therefore, we compare the regime variability of the reconstructed data with that of a 500-year long, externally forced model simulation (Zorita et al. 2004). Before that, the corresponding control run was analysed with respect to regime variability (Handorf et al. 2004) presenting hints on multi-model regime behaviour.

This study is organised as follows. In Section 2, the two data sets are introduced. Section 3 presents the methodology used to detect recurrent climate regimes in the 500 hPa geopotential height fields. Section 4 deals with the leading patterns of climate variability for the North Atlantic/European sector 1659–1990. Section 5 depicts the reliability of reconstructed data in reproducing recurrent climate regimes. Moreover, the recurrent climate regimes for the reconstruction and the model are presented for the period 1659–1990. Finally, the temporal evolution and the potential of both the data sets in reproducing recurrent climate regimes is discussed. Conclusions are given in Section 6.

2 Data

2.1 Reconstructed 500 hPa geopotential height fields

Luterbacher et al. (2002) statistically reconstructed monthly means of the 500 hPa geopotential field from 1659 to 1990 and seasonal means from 1500 to 1658 for the area 70°N–30°N to 30°W–40°E on a 2.5°×2.5° grid.

Instrumental station temperature, pressure, and precipitation series in combination with documentary proxy evidence (e.g. Glaser et al. 1999; Pfister 1999) from various European areas are used in what is termed a ''reverse specification'' (Klein and Dai 1998) to statistically reconstruct the 500 hPa geopotential height fields. A principal component regression analysis is used to derive the statistical relationships between the climate information (predictors) and the NCEP-reanalysis data (Kalnay et al. 1996; Kistler et al. 2001) during the calibration period 1948–1990. Luterbacher et al. (2002) applied different calibration/verification exercises within that period in order to obtain information on the stability of the results and the quality of the reconstructions through time. The transfer func-

tions obtained over the 1948–1990 period were applied to the pre-1948 data in order to get the final estimates of the mid-tropospheric fields back to 1500. For details of the reconstruction technique, the sources of the predictor data, and the uncertainties, the reader is referred to Luterbacher et al. (2002).

The methodology for the reconstruction is based on the assumption of stationarity. Thus, the statistically derived relationships between the combined station time series and the large-scale 500 hPa geopotential height fields over the calibration period remain the same through the reconstruction period.

Reduction of error (RE) statistics (see Cook et al. 1994 for a review) were calculated grid point by grid point between the NCEP-reanalysis data and the estimations during the verification period 1976–1990. Figure1 presents the evolution of the spatially averaged RE-values over all 435 grid points for the North Atlantic/ European sector for the winters (DJF) 1500–1990. RE ranges from +1 (perfect agreement between reconstructions and observed time series for the verification period) to ∞. RE = 0 means that the reconstruction is no better than climatology (i.e., the mean of the period 1948–1990). Negative values indicate that the reconstruction provides no useful information. The reconstruction data show good skill for the period 1659–1990. It can be seen that for the period 1500–1658 the RE-values averaged over the entire North Atlantic/European grid are rather low and therefore, only the data from 1659 onwards are used for the detection of the climate regimes. The lowered overall quality can be attributed to the limited climatic information from only a few predictors without pressure information for the pre-instrumental period. From 1659 onwards, the quality of the reconstruction increases with time similar to the number of predictors, especially when station pressure series become available.

2.2 Modelled 500 hPa geopotential height fields

The modelled data set were obtained from a transient 500-year integration of the coupled atmosphere–ocean general circulation model ECHAM4/HOPE-G (ECHO-G; Legutke and Voss 1999) with prescribed time-evolving external forcing functions (Zorita and González-Rouco 2002; Zorita et al. 2004). These external forcing functions are based on the historical values of the solar constant, including volcanic activity through changes of the effective solar constant (Crowley 2000), of the CO_2 concentration (Etheridge et al. 1996) and of the CH_4 concentration (Blunier et al. 1995) for the period 1500–1990.

The ECHO-G consists of the atmospheric GCM ECHAM4 (Roeckner et al. 1996) and the global version of the Hamburg ocean primitive equation GCM HOPE-G (Wolff et al. 1997). The atmospheric model is based on the full set of the primitive equations. Processes like radiation, clouds, precipitation, convection, and diffusion, have been parameterised. Nineteen sigma pressure levels reaching from the ground up to 10 hPa give the vertical resolution of the atmosphere. The horizontal spectral resolution of T30 corresponds to a Gaussian grid of 3.75°×3.75°. The oceanic GCM includes 20 vertical layers and has a horizontal resolution of T42 (2.8°×2.8°) with further meridional refinement up to 0.5° in the equatorial region. Furthermore, it incorporates a dynamic–thermodynamic sea–ice model with snow cover. For the long-term simulation, an annual-mean flux correction for heat and fresh water is applied to avoid an unrealistic climate drift of the coupled system.

In agreement with the reconstructed data, our study on the behaviour of tropospheric circulation regimes over the North Atlantic/European sector has been determined on the basis of monthly mean winter (DJF) data for the region 70°N–30°N to 30°W–40°E.

Fig. 1 Model performance (reduction of error; RE) for the reconstructed winter (DJF) 500 hPa geopotential height fields plotted against the time for which a given multivariate model (for the verification period 1976–1990) was used. The RE is the spatial average over 435 grid points over the North Atlantic/European sector. The calibration/ verification (1948–1990; C/V), the reconstruction (1500–1947), and the studied period 1659–1990 are marked by arrows
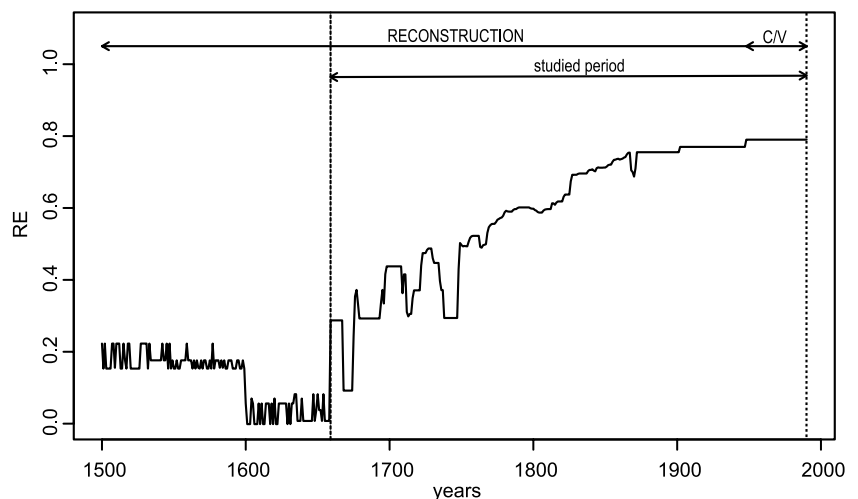
3 Methods

In Section 1, climate regimes were introduced in a general sense as recurrent/persistent circulation patterns. Accordingly, climate regimes are defined in terms of the PDF of the 2-dimensional reduced sub-space as patterns, which correspond to areas of the state space with an unexpected high recurrence probability. The basis of this study is a monthly mean winter (DJF) data of 500 hPa geopotential height for the North Atlantic/European sector, characterising the flow of the free atmosphere.

The method to determine climate regimes comprises the reduction of the state space to the two leading basis functions. Further, it includes the estimation of the PDF of this state space. Then, areas of the state space with an unexpected high recurrence probability are detected and finally, spatial patterns of the recurrent climate regimes are calculated.

Similar to the studies of Kimoto and Ghil (1993a, 1993b), Corti et al. (1999) and Hsu and Zwiers (2001), the reduced state space is spanned by the two leading EOFs. Joint EOFs have been calculated on the basis of the combined data sets of modelled and reconstructed data over the North Atlantic/European sector to regard the same state space for the reconstructed as well as for the modelled data and thus, to ensure good comparability of the PDFs.

The EOF patterns are calculated on the basis of the monthly anomaly winter data after removing the seasonal cycle and correcting for latitudinal distortions. Afterwards, all EOF patterns are re-normalised by the square root of the corresponding eigenvalues. Thus, the re-normalised EOF patterns carry the units of the data and the corresponding time series (principal components; PCs) are standardised (cf. von Storch and Zwiers 1999). The state variables of the reduced state spaces either for the modelled or for the reconstructed data are formed by the so-called Pseudo-PCs, obtained by projecting the corresponding data onto the two leading joint EOFs. Therefore, the statistical properties (mean, variance and autocorrelation) of the Pseudo-PCs are slightly different from those of the regular PCs.

The joint PDF p(PC1 and PC2) of the state space is calculated with a non-adaptive Gaussian kernel estimator (Silverman 1986). For this kind of computation, the properties of the kernel estimator strongly depend on the smoothing parameter h. To avoid the pretence of multimodality of the PDF we use the optimal window width h_{opt} for normally distributed data with unit variance according to Silverman (1986). The optimal window width ensures the minimising of the mean integrated squared error and is given by

$$h_{opt} = A \times n^{-1/d+4}$$

with n length of time series, d dimensionality and $A = 0.96$ for $d = 2$ and a Gaussian kernel.

The optimal window width h_{cro} for the analysed, not necessarily normally distributed data, can be determined by a least-squares cross validation method to minimise the mean integrated squared error (score function) between the "true" and the estimated density (Silverman 1986). For the data sets used in this study, the score function revealed a broad minimum, and the differences between h_{opt} and h_{cro} are rather small (between 5% and 25%) and the detected climate regimes remain the same for h_{opt} and h_{cro} (not shown). These results are similar to those of Hsu and Zwiers (2001), for observed northern hemispheric data. In the following, the data-independent value of $h = h_{opt}$ is chosen for all PDF calculations instead of the cross-validated value, again in order to ensure good comparability between the PDFs.

Areas of the state space with an unexpected high recurrence probability are estimated by means of adequate Monte Carlo (MC) simulations (e.g. Kimoto and Ghil 1993a, 1993b). Therefore, 1000 random pairs of Pseudo-PC time series are simulated with the same mean, variances, lag-one autocorrelation and correlation coefficients as the original Pseudo-PC time series (PC1 and PC2). The areas with an unexpected high recurrence probability are defined by using the 95% (90%) confidence interval, i.e., 950 (900) or more simulated PDFs have smaller probability values than the original PDF at these regions.

To support the robustness of the determined preferred regions of the state space the difference between the joint PDF p(PC1 and PC2) and the product of the marginal PDFs p(PC1) × p(PC2) is investigated. In the case of statistically independent Pseudo-PCs this difference would be identical to zero, otherwise the Pseudo-PCs are statistically dependent. Areas with positive values of this difference represent preferred regions of the state space. It is worth mentioning that studies by Monahan et al. (2001) even confirm the coincidence of these regions with regimes determined by means of a nonlinear generalisation of principal component analysis.

To fully characterise the significance of the determined regimes, the local significance test that is described is not sufficient. According to Hsu and Zwiers (2001), a global test quantity IPDF is defined as the integral of the estimated PDF over the estimated preferred regions of the state space. Thus, a low value of IPDF suggests that the estimated preferred regions are connected with small residence probability and may not be indicative for recurrent regimes. Again, the significance of the IPDF is determined by the previous MC simulations, taking into account those MC simulations, which have an IPDF smaller than that of the estimated PDF from our data. This test statistic p(IPDF) takes into account whether the areas of an unexpected high recurrence probability are connected with relatively high PDF values and give (for high values) evidence that the determined regimes are not regimes resulting from sampling variability.

4 Leading patterns of climate variability

The dominant joint spatial patterns of the reconstructed and modelled winter (DJF) data over the North Atlantic/European sector from 1659 to 1990 are displayed in Fig. 2. The first two EOFs accumulate approximately 54% of the total 500 hPa winter geopotential variance. The most dominant pattern (Fig. 2, left panel, explaining 29.1% of the variance) shows a monopole structure centred over the British Isles, which depicts the existence of blocking anticyclones (in case of positive PC values) or troughs (in case of negative PC values). The second EOF (Fig. 2, right panel, explaining 24.9%) resembles a NAO−like dipole-structure with a northward shift of the centres of action. The first two leading EOFs are well separated after North's rule-of-thumb (North et al. 1982) from EOF3. Note that an EOF analysis on the reconstructed and modelled data separately revealed similar patterns (not shown). This includes a blocking pattern (EOF2 of the reconstructed and EOF1 of the simulated data) and a dipole, NAO−like pattern (EOF1 of the reconstructed and EOF2 of the simulated data). The latter differ with respect to the orientation of the dipole axis, it is NW–SE oriented for the reconstruction, and NE–SW oriented for the simulation.

To analyse the temporal evolution of these circulation patterns, a continuous wavelet transformation is applied to the Pseudo-PC time series for both the reconstructed and modelled data. By using this transformation (e.g. Kumar and Foufoula-Georgiou 1997; Torrence and Compo 1998), it is not only possible to determine the dominant periods of a time series, but also their occurrence time. Thus, more information about the non-stationary behaviour of time series is gained.

Figures 3 and 4 show the time series of Pseudo-PC1 (left panels, a and c) and Pseudo-PC2 (right panels, b and d) for the reconstructed and modelled data, respectively. The most striking feature is the good resemblance of the behaviour of the NAO for the last decades with the evolution of Pseudo-PC2 of the reconstructed data (Fig. 3b). This time series shows the pronounced period of negative NAO−values (accordingly negative Pseudo-PC2 values) in the 1960s followed by an increased frequency of positive NAO phases in the 500 hPa geopotential fields (e.g. Hoerling et al. 2001; Hurrell et al. 2004). Furthermore, the range of variability of the Pseudo-PC2 increases significantly around 1770. After that time the RE-values, describing the quality of the reconstructions, reveal highly skilful reconstructions (cf. Fig. 1). The simulated data (Fig. 4b) show only a slight tendency to increased PC2 values corresponding to an increased frequency of positive NAO phases for the last 10 years. The model does not reproduce the period of negative NAO−values in the 1960s.

The inspection of the blocking-related Pseudo-PC1 reveal for the reconstructed data rather small variations on the decadal timescale (cf. filtered time series) except a period of about 30 years from 1670 to 1700 with pronounced positive values of Pseudo-PC1. This persistent occurrence of blocking situations is connected with enhanced inflow of cold polar air to central Europe during that time (Wanner et al. 1995; Luterbacher et al. 2001). This feature is not visible in the model data.

In the lower panels of Figs. 3 and 4, the local wavelet power spectra, obtained with the Morlet wavelet, depict variability at interannual, decadal and interdecadal timescales. For the Pseudo-PC2 of the reconstructed data, which correspond to the NAO, we
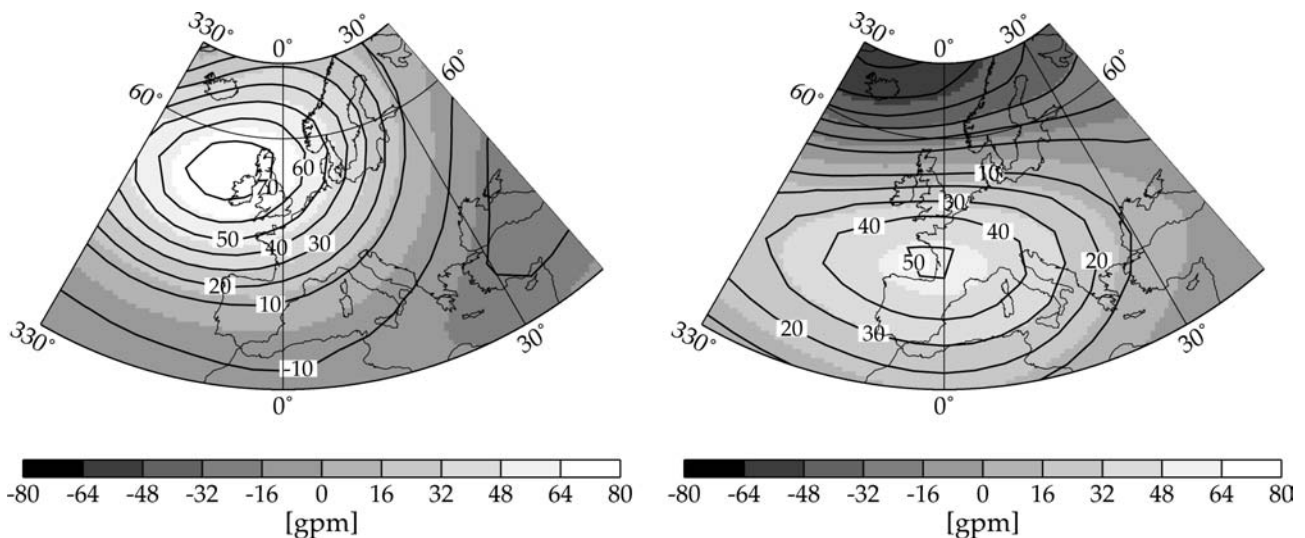

Fig. 2 The first two joint empirical orthogonal functions (EOFs) based on the combined data sets of modelled and reconstructed data over the North Atlantic/European sector. Data are monthly mean winter (DJF) 500 hPa geopotential height fields from 1659 to 1990. EOF1 (*left panel*) explains 29.1%, EOF2 (*right panel*) 24.9% of the total variance

Fig. 3 *Upper panels*: unfiltered
(*black*) and smoothed (*white*,
10-year Gaussian filter) time
series of Pseudo-PC1 (**a**) and
Pseudo-PC2 (**b**) of the monthly
mean reconstructed winter
(DJF) 500 hPa geopotential
height fields from 1659 to 1990.
c, d Corresponding local
wavelet power spectra, obtained
with the Morlet wavelet. At
both ends, *dash-dotted* lines
separate regions where edge
effects become important. The
thick contour envelopes areas
exceeding the 95% confidence
level for a corresponding red
noise process
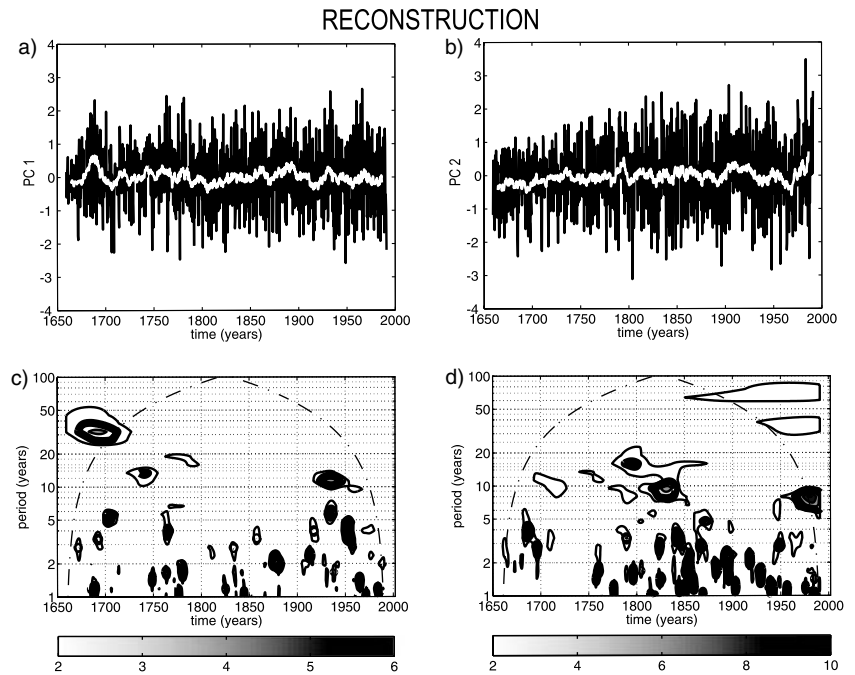
have found significant signals for periods about 6–8 years for the last 50 years (cf. Fig. 3d). Again, this coincides with findings from the observational NAO−record (Hurrell and van Loon 1997; Handorf et al. 1999). The Pseudo-PC2 time series for the modelled data have not revealed increased variability on the interannual timescale, but increased variability at interdecadal periods about 40–50 years for the first half of the considered period 1659–1990 (Fig. 4d). The blocking time series for both, the reconstructed and modelled data (Pseudo-PC1, Figs. 3c and 4c), display a rather random behaviour with largest variations before

1750 in accordance with the above described variations.

5 Recurrent climate regimes and temporal evolution

5.1 Reliability of reconstructed recurrent climate regimes 1948–1990

In order to investigate the reliability of reconstructed data for the determination of recurrent climate regimes, the period from 1948 to 1990 is investigated. Note that

Fig. 4 Same as in Fig. 3, but
for monthly mean winter (DJF)
modelled data from 1659 to
1990
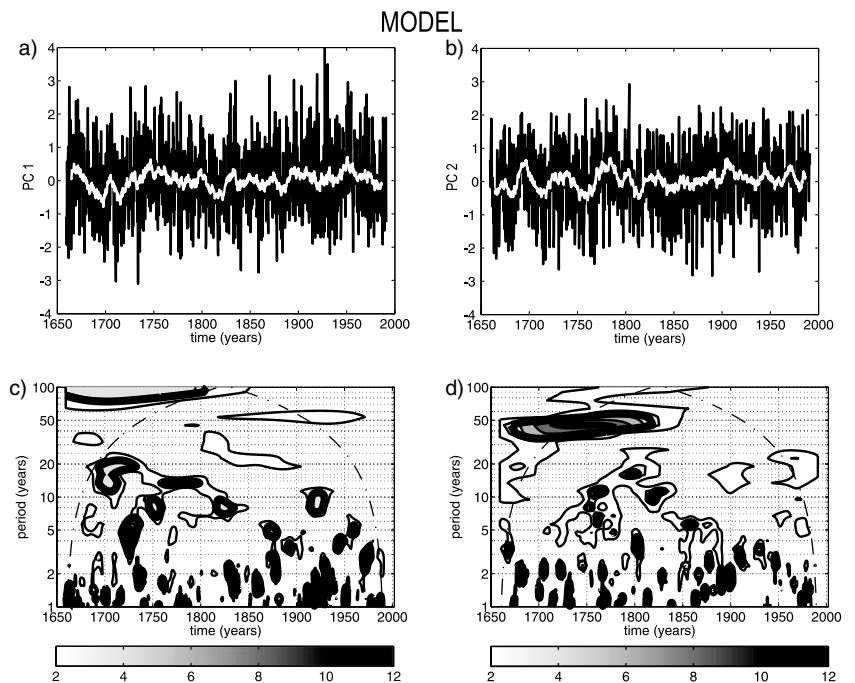
reconstructions of the calibration period are used for this period. In Luterbacher et al. (2002), the data from 1948 onwards is the reanalysis itself. The reconstructed data are of high quality during that time (cf. Fig. 1) and compared with the NCEP reanalysis (Kalnay et al. 1996; Kistler et al. 2001). According to the described methodology, the basis of the reduced state space is formed by the first two joint EOFs of the reconstructed and the NCEP reanalysis 500 hPa geopotential height fields for DJF.

The structure of these EOFs differs from that of the period 1659–1990. The joint EOF1 1948–1990 (26.5%) reveals a NAO−dipole, which differs from EOF2 for the whole period (right panel Fig. 2) by its orientation. EOF2 (26.2%) is very similar to the blocking EOF1 for the whole period (left panel Fig. 2).

Figure 5 presents a comparison between the PDFs of the NCEP reanalysis Pseudo-PCs (Fig. 5a) and the reconstructed Pseudo-PCs (Fig. 5b) 1948–1990. The PDFs are calculated using the optimal bandwidth 0.43.
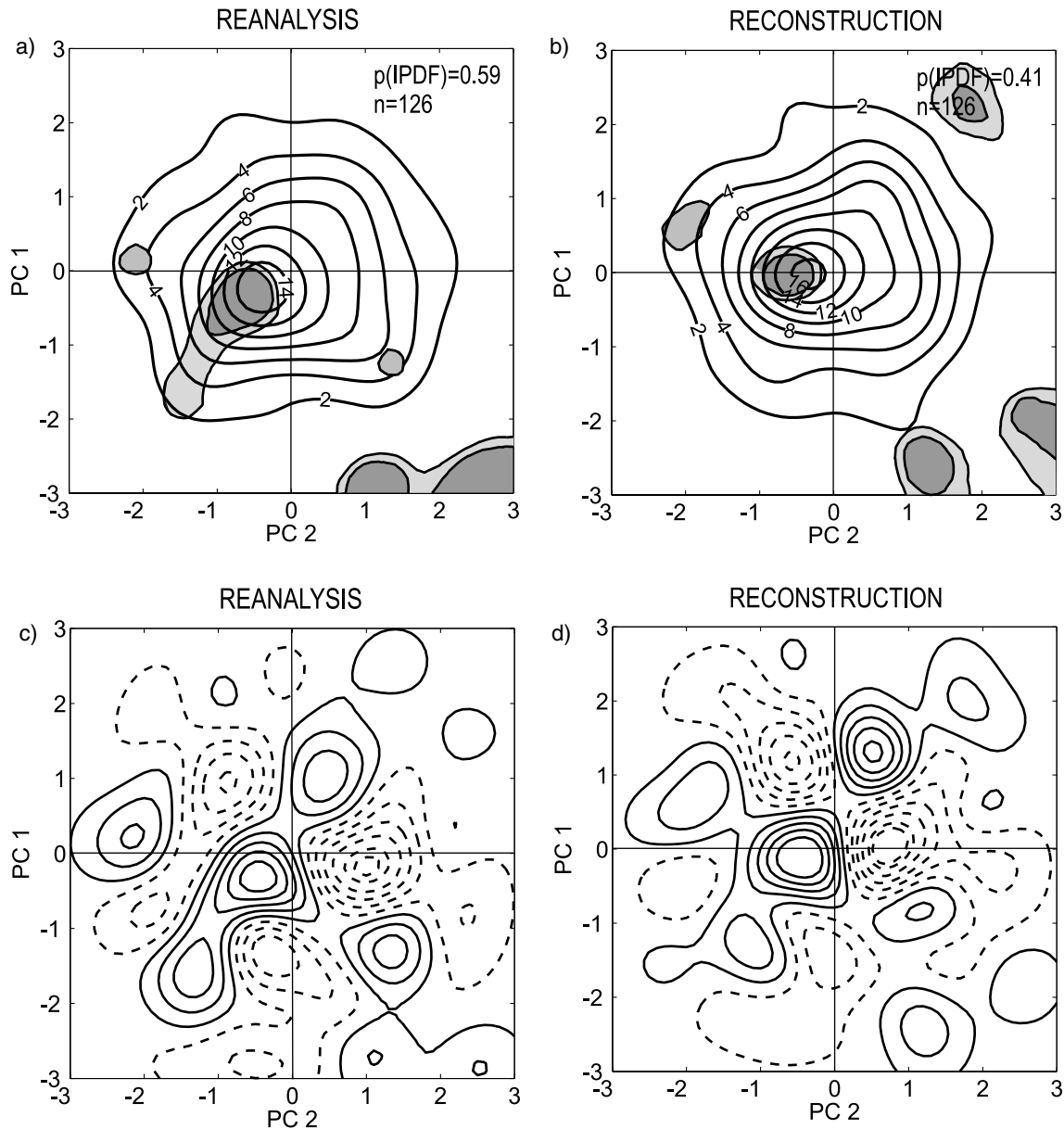

Fig. 5 Probability density function (PDF, contours in %) for monthly mean of winter (DJF) NCEP reanalysis data (a) and reconstruction data (b) from 1948 to 1990 in the state space spanned by the first two joint EOFs. *Light grey shaded* areas mark regions with an unexpected high recurrence probability on a confidence level of 90%, *dark grey shading* reveals the 95% level. Both are determined by means of a MC approach. The PDFs are calculated with the optimal bandwidth 0.43. The value given by p(IPDF) is the probability that the global test quantity p(IPDF) is greater than the corresponding value of random MC simulations on the 95% confidence level. Difference plots are plotted between the joint PDF p(PC1,PC2) and the product of the marginal PDFs p(PC1) × p(PC2) for monthly mean winter (DJF) NCEP reanalysis data (c) and reconstructed data (d) from 1948 to 1990. The *solid lines* mark positive values indicating preferred regions in the PDF, the *dotted lines* show the negative values (contours are +/−0.2, 0.6, 1, 1.4, 1.8)
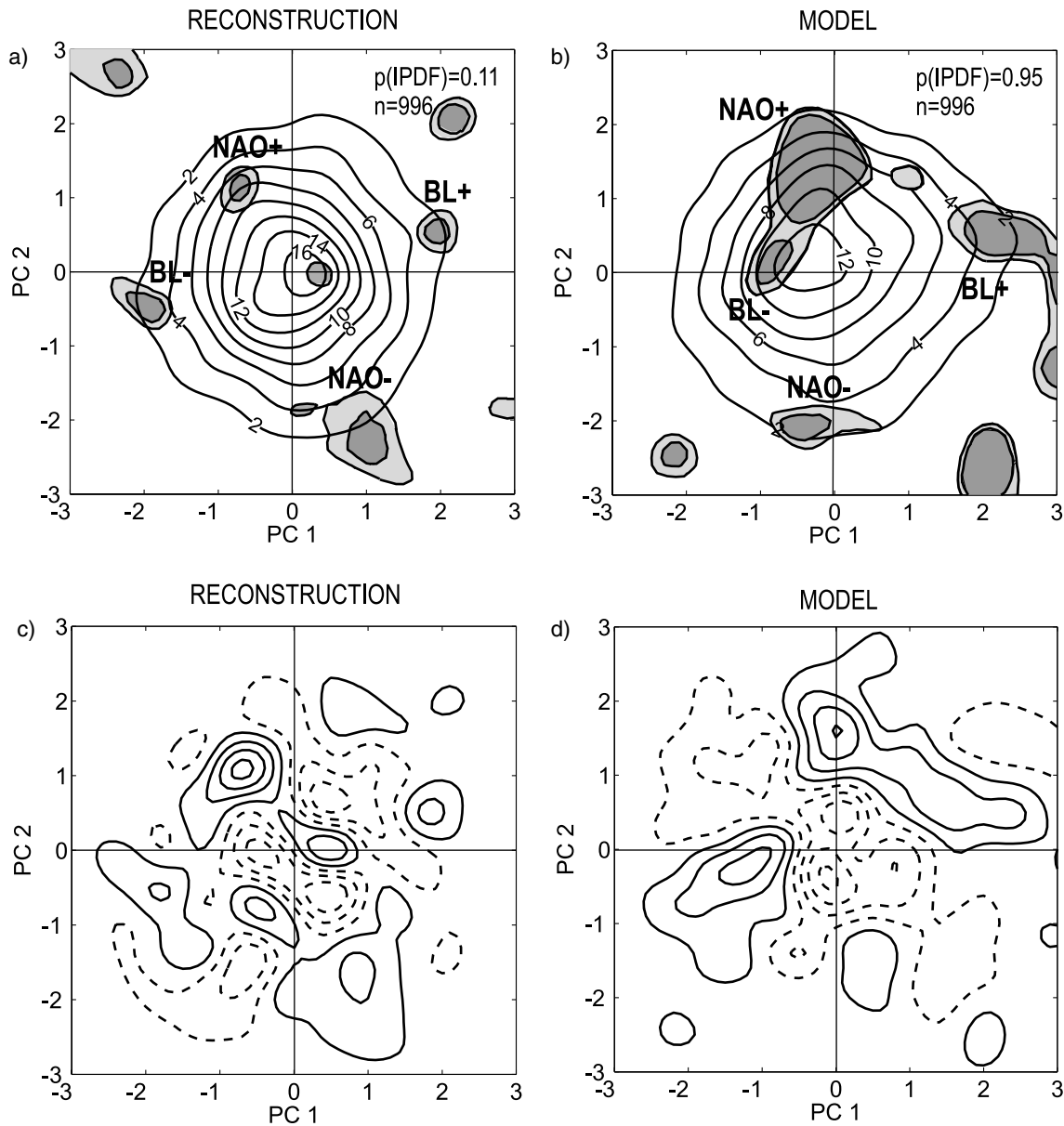
Fig. 6 Same as in Fig. 5, but for monthly mean winter (DJF) reconstructed (**a, c**) and modelled (**b, d**) geopotential height fields from 1659 to 1990. The optimal bandwidth is 0.3

Regions of unexpected recurrence probabilities are indicated by shaded areas and denote recurrent climate regimes. These regions are derived using the described MC approach on the 90% and 95% confidence level. Additionally, Fig. 5c (Fig. 5d) displays the differences between the joint and the product of the marginal PDFs (difference-PDF) for the NCEP reanalysis (reconstruction). Positive values are indicated by solid lines and represent preferred regions of the state space; areas with negative values of the difference are enclosed by dashed lines.

The MC approach for the NCEP data (Fig. 5a) reveals one dominant regime on the 95% confidence level and for PDF-values $>2\%$. It is located at the centre and

stretched towards the edge of the PDF. The comparison with its difference-PDF (Fig. 5c) suggests that this region of unexpected high recurrence probability corresponds to two regimes, one located near the centre of the distribution and the other located in the lower left quadrant at the edge of the distribution. For the reconstructed data (Fig.5b), one dominant regime located at the centre of the distribution is detected on the 95% confidence level. The comparison of the difference-PDF (Figs. 5c and d) reveals a very similar structure concerning the position of the five maxima and four minima in the state space (for the region of PDF-values $>2\%$) for the two data sets. The joint examination of PDF and difference-PDF leads to the conclusion that for the NCEP data as well as for

the reconstructed data the general structure of the PDF is very similar. The significant recurrent regime located near the centre of the distribution is reproduced by both data sets. The fact that the regimes detected at the edge of the distributions do not pass the MC based significance test can be attributed to the rather small sample size of 126 (42 winters). The values for the global test statistics p(IPDF) (0.59 for NCEP-data and 0.41 for reconstructed data), indicate that the overall evidence for recurrent regimes for the North Atlantic/European sector is sufficient for the period 1948–1990.

To summarise, the analyses of this section revealed similar results for NCEP as well as reconstructed data concerning the structure of the PDF, the positions of the regimes in the state space and the overall evidence for recurrent regimes. Thus, for the period 1948–1990 (and periods of similar quality) reconstructed data can be reliably used for the determination of recurrent regimes; however, the p(IPDF) is lower for the reconstruction than for the reanalysis.

5.2 Recurrent climate regimes for the period 1659–1990

Figure 6 shows the PDFs of the reconstructed and modelled monthly mean winter data of the 500 hPa geopotential height fields for 1659–1990 in the state space spanned by the first two joint EOFs. The PDFs are calculated using the optimal bandwidths of 0.3. Therefore, the PDFs are directly comparable. Again, regions of unexpected recurrence probabilities are derived using the MC approach and indicated by shaded areas. As in Fig.5, the difference-PDFs are displayed in the lower parts of Fig. 6.

For the reconstructed data, four significant regions are detected by means of the MC simulations on the 95% confidence level (Fig. 6a). Only regimes within PDF-values > 2% are considered. The position of these recurrent climate regimes in the state space is confirmed by the difference-PDF displayed in Fig. 6c. For the modelled data (Fig. 6b), the MC approach on the 95% confidence level reveals also four regions of unexpected recurrence probability. In accordance with the structure of the EOFs spanning the state space, the four regimes are lettered by NAO+, NAO−, BL+ and BL−. On the 95% confidence level, the significant regions related to the NAO− and BL+ regime are situated at similar regions of the state space in both the data sets. The NAO+ and BL− regimes are detected at somewhat different state space regions. The additional fifth regime, for the reconstructed data, on the 90% confidence level is not considered here in detail due to its position near the centre of the distribution corresponding to a frequent occurrence of the mean circulation. This is due to an overestimation of mean conditions of the reconstruction algorithm for periods with lowered skill (prior to 1700, cf. Fig. 1). For the reconstruction, the assumption of normal distributed residuals is made.

Thus, the higher the residuals due to a low number of predictors, the more the reconstruction tends to normal distribution.

The main difference between the modelled and reconstructed data is related to the overall evidence for recurrent regimes. The values for the global test statistics p(IPDF) amount to 0.11 for the reconstructed data and to 0.95 for the modelled data. Thus, for the period 1659–1990, the overall confidence for recurrent regimes is high only for the model.

For a physical interpretation, an anomaly composite of each reconstructed (modelled) recurrent climate regime is presented in Figs. 7 and 8a–d. These anomaly composites are obtained by averaging all geopotential height anomaly fields (members) belonging to the state space range of recurrent climate regimes characterised in Figs. 6a and b by the dark-grey shaded areas. Furthermore, the standard deviations for each regime are calculated as a measure for the variability of all members that form a composite.

The BL+ regime (Fig. 7a, consisting of four members) for the reconstruction exhibits a typical European blocking dipole with strong positive geopotential height anomalies over northwestern Europe and the adjacent North Atlantic and negative ones for the Mediterranean and eastern Europe. This configuration blocks storm activity from the North Atlantic and is connected with anomalous northerly flow towards central Europe. The reconstructed BL+ regime indicates strong similarities to the modelled BL+ (Fig.8a, 22 members). Distinctions are found in the distribution of the standard deviation. The composite of the reconstructed BL+ shows higher variability than the modelled BL+. High values occur in both regimes along a ridge from the Baltic Sea towards the Mediterranean. The highest values for the reconstruction are found over the western North Atlantic.

The BL- regime for the reconstruction is the opposite pattern of BL+ (Fig. 7b, ten members). Generally, the BL- regime composite for the reconstructed data has stronger anomalies compared with the corresponding modelled regime (Fig. 8b, 52 members). The distribution of the standard deviation is similar in both composites, showing high values in the central North Atlantic and over western Russia.

The NAO+ regime for the reconstruction (Fig. 7c, 31 members) presents a dipole structure with negative geopotential height anomalies centred over Iceland and positive values extending from the Azores to the central Mediterranean. This is connected with strong westerly mid-tropospheric flow towards Europe. The modelled NAO+ regime (Fig. 8c, 109 members), which is also significant on the 99% confidence level, shows a similar structure as its counterpart in the reconstruction. However, the southern centre of action is shifted northwards. The standard deviation pattern is similar in both regimes, though developed stronger in the modelled anomaly composite.

The reconstructed NAO− regime (Fig. 7d, nine members) is the inverse pattern of Fig. 7c. It is connected
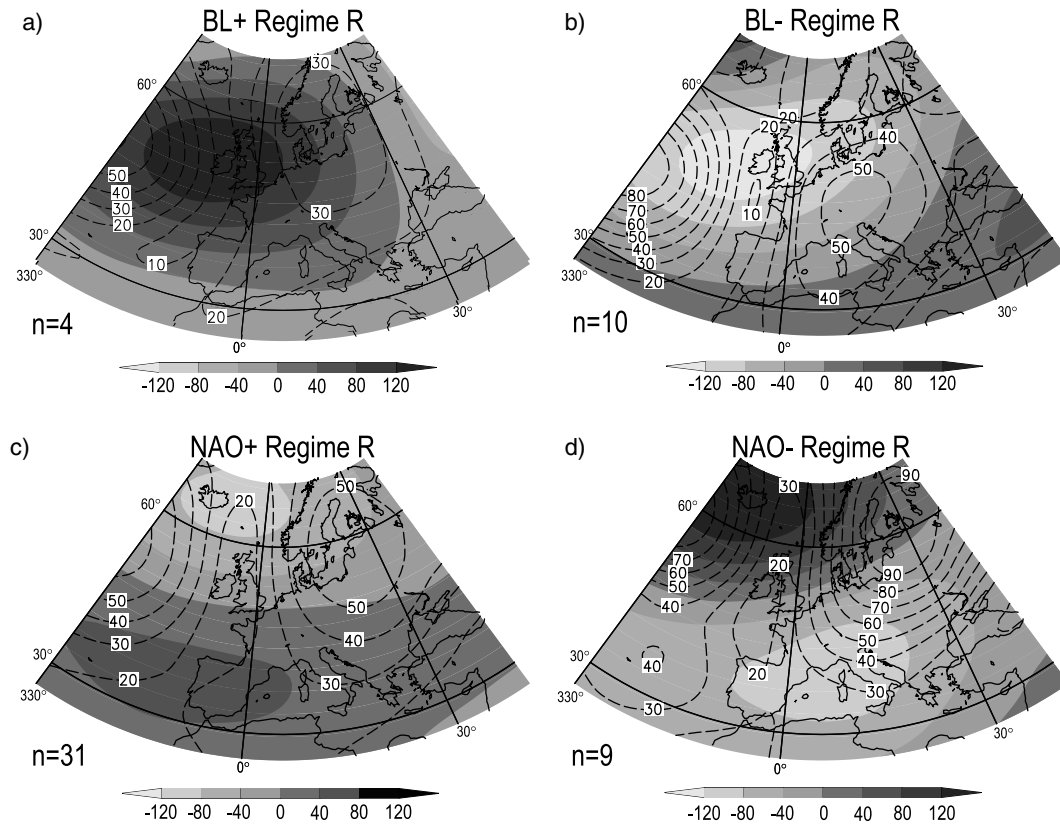
Fig. 7 a–d Anomaly patterns of reconstructed 500 hPa geopotential height fields (in gpm, shaded) of the winters (DJF) belonging to the four recurrent climate regimes detected on the 95% confidence level (*dark grey shading* in Fig. 6a). The *dotted contours* indicate the standard deviation for the patterns

to a weakening of the Icelandic Low and the Azores high. The decreased geopotential height difference leads to a weakened zonal flow towards Europe. The NAO− regime for the reconstruction differs slightly from the modelled composite (Fig. 8d, 12 members). For the modelled NAO−, the positive centre of anomalies is shifted eastwards, the negative centre northwards and expands towards the North Atlantic. The distributions of the standard deviations reveal more similarities, with two centres of maxima in the central North Atlantic and northeastern Europe. The variability of the reconstructed NAO− regime is higher than for the modelled data.

To summarise, the analyses revealed four significant recurrent climate regimes for the reconstruction and the model data. However, for the period 1659–1990, the overall confidence for recurrent regimes is high only for the model. The composite analysis shows that these regimes are related to the two phases of the NAO and the two opposite blocking situations.

5.3 Temporal evolution of recurrent climate regimes

The length of the two data sets allows to improve the understanding in the temporal evolution of the North Atlantic/European recurrent climate regimes for the last 331 years. For both the data sets, the Pseudo-PCs are divided into running windows, covering 100 winters each, and the corresponding PDFs for these segments are estimated. The PDF of the first running window segment is, therefore, calculated by the two leading Pseudo-PCs of the winters 1659–1758, the second from 1660 to 1759 and so on. The temporal evolution of the global test quantity p(IPDF) of the recurrent climate regimes is presented in Fig. 9 in order to investigate the evidence for climate regimes in the two data sets over time. Furthermore, two animations of the temporal recurrent climate regime evolution are provided (see *Electronic Supplementary Material* ''reconstruction.gif'' and ''model.gif''). In the first pictures of these animations, all segments are plotted on top of each other to visualise preferred regions for the occurrence of regimes in the PDF.

The p(IPDF) values for the modelled geopotential height field regimes (solid lines) are generally higher than for the reconstruction (dashed lines) for the period after 1720 (+/−50 years). Regarding only these two realisations of the past climate for the North Atlantic/European sector, the model reveals more evidence of recurrent climate regimes than the reconstruction. However, it is questionable, which realisation is more realistic. Therefore, we assess the evolution of the time series using independent evidences (i.e. data that are not used for the reconstruction and the validation of the model) of past circulation flow over the studied area.
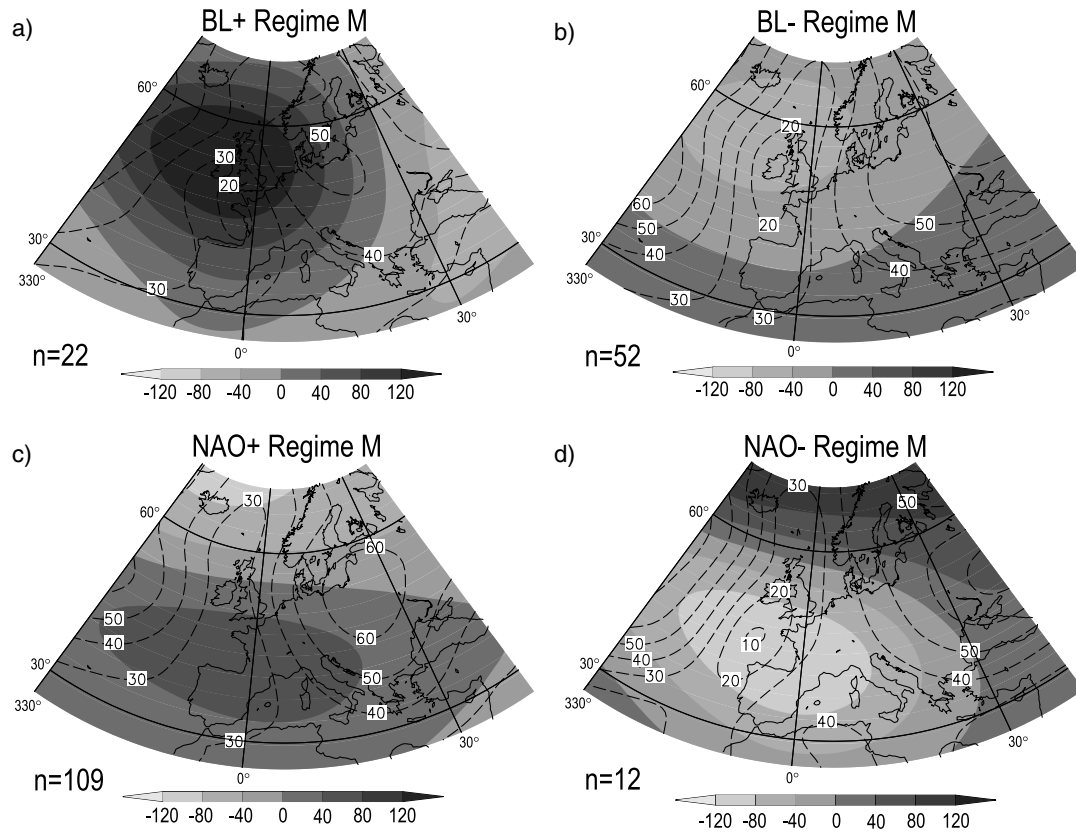
Fig. 8 a–d The same as in Fig. 7, but for the the four regimes detected in Fig. 6b for the model data

From 1670 to 1700, the reconstruction reveals a period with a persistent occurrence of blocking situations (Fig. 3a), which is not represented by the modelled data (Fig. 4a). Koslowski and Glaser (1999) report a phase of sea–ice extension in the Western Baltic that is strongly connected to weak westerlies and the existence

Fig. 9 The temporal evolution of the global test statistic value p(IPDF) for the running window segments, covering 100 winters each, starting 1659–1758. The solid line marks the p(IPDF) values for the model, the dotted line for the reconstruction. The p(IPDF) values are calculated on the basis of the 95% confidence level

of persistent blocking situations over Europe during that period. The reconstruction shows a strong BL+ regime at central position of the PDF in combination with a dominant NAO− regime during that period (see *Electronic Supplementary Material* "reconstruction.gif"). The skill of the reconstructions is reduced prior to 1720 (Fig. 1) and this may lead to an overestimation of normal distributed reconstructions and the appearance of the BL+ regime near the centre of the PDF. The PDF exceeds in its central position values of 20%, whereas the model reveals highest PDF values of around 10%. After 1720, the BL+ regime at the central position vanishes. This also explains the rather high p(IPDF) for the reconstruction prior to 1750.

The p(IPDF) values for the reconstructed recurrent climate regimes are generally very low during the period 1770–1830. This period is characterised by a prominent transition of the regimes (see the animation for the reconstruction). The BL+ regime completely disappears, the dominant NAO− regime is weakened and around 1790 (+/−50 years) the NAO+ regime becomes the dominant pattern. This can be traced back to the positive peak in the NAO related Pseudo-PC2 of the reconstruction around 1770–1800 (Fig. 3b). Slonosky et al. (2000) reported an increased meridional flow over central Europe (e.g. Paris–London Index) during that time. This period is often referred to as the Dalton Minimum, a decrease in the solar irradiance from around 1790 to 1830. It is beyond the scope of this study
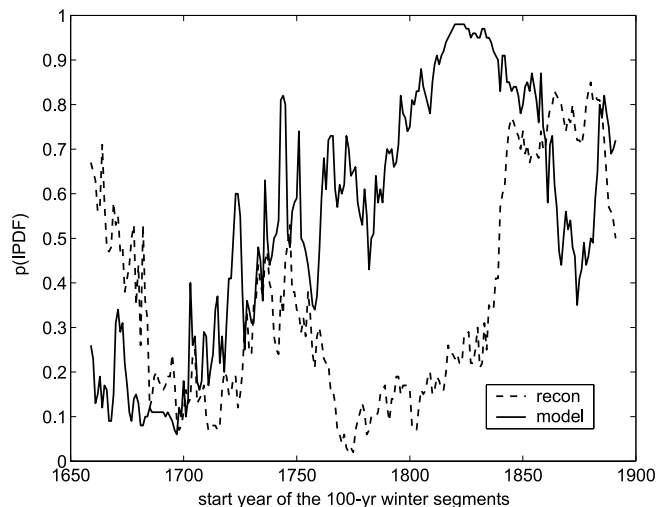
to relate the low p(IPDF) values of the reconstruction to a decrease in solar forcing. However, the quality of the reconstruction for this period is highly skilful (cf. Fig 1) and cannot explain the decrease in the p(IPDF) quantities.

After 1850, the modelled and the reconstructed data show high p(IPDF) values. The animation for the reconstruction reveals four regimes; however, the NAO + regime dominates. This is related to the realistic trend of positive Pseudo-PC2 values after 1960 (Fig. 3b). This is not that evident for the model. It also shows a dominant NAO + phase, but in interaction with the BL + regime.

Regarding the two animations and especially their first pictures, it becomes clear that regimes appear at preferred regions in the PDF and that there are regions, which are never occupied. Except the central BL + regime for the reconstruction prior to 1720, all these regimes seem to be robust but temporally variable. They appear mainly at the positions already detected in Figs. 6a, b (shaded areas).

To summarise, the evolution of recurrent climate regimes is not stable over time. Generally, a better evidence of recurrent climate regimes is found in the model for the period after 1720 than in the reconstruction. However, there are some indications that the reconstruction reproduces more realistic regimes for the North Atlantic/European sector after 1720, when compared with the independent evidence of past climatic anomalies. Prior to 1720, a BL + regime at central position of the state space for the reconstructions is detected, which is not robust over the whole period. It appears mainly due to the lowered quality of the reconstruction. The higher degree of realism on the side of the reconstructions suggests that the chronological evolution of the regimes on these timescales in this model realisation is rather related to the internal variability in the climate system than to the changes in external forcing factors used to drive the model, the only link of the model to the past. This interpretation is supported by analysis of the control simulations (Handorf et al. 2004) revealing climate regimes without any changes in the variations of the external forcings.

6 Conclusions

The detection of recurrent climate winter regimes in reconstructed and modelled 500 hPa geopotential height fields over the North Atlantic/European sector 1659–1990 is presented. Recurrent climate winter regimes are defined as patterns, which correspond to areas of a low-dimensional, reduced state space with an unexpected high recurrence probability. In order to consider a comparable state space, the modelled and reconstructed data are combined.

The detection of recurrent climate regimes is achieved by using an appropriate MC technique. The method for estimating the PDF is sensitive to the selection of an adequate bandwidth and the choice of the kernel function. In this study, optimal values for the bandwidth are determined to avoid spurious multimodality and ensure the comparability of the PDFs. Furthermore, a global test statistic is introduced.

The reliability of the reconstructed recurrent climate regimes is investigated by comparing reconstructed 500 hPa geopotential height fields for the winters 1948–1990 with NCEP reanalysis data. The regime detected in the reconstruction is similar to the one in the reanalysis. Similarities are also found for the structure of the underlying PDF. It is stated that the reconstructed data are reliable for the determination of recurrent regimes during the period 1948–1990 and during periods with similar quality of reconstructed data.

Both, the statistically reconstructed and the modelled data for the observed geographical sector show low-frequency variability in the form of recurrent climate regime characteristics during the winters 1659–1990. Four similar regimes for both the data sets are detected. The composite analysis shows that these regimes are related to the two phases of the NAO and two opposite blocking situations reflecting the most important patterns of atmospheric variability for the North Atlantic/European sector for the period 1659–1990.

A running window, covering 100 winters each, is applied to the PCs and the corresponding PDFs are estimated in order to investigate the temporal evolution of the climate regimes. There is more evidence for recurrent climate regimes in the modelled data due to the generally higher values of the global test statistics for the period 1720 onwards. However, the detected chronology of regimes for the reconstruction is supported by findings from independent data sources.

Spatio-temporal reconstructions as the one analysed here offer long and high-quality estimations of past climate variability. Combined studies of reconstructions and model output help improve our understanding of past climate dynamics and processes, when considering their limitations and uncertainties. The investigated specific model simulation of ECHO-G reveals the same climate regimes as the reconstruction, but differences with respect to the regime chronology are found. At this point, we see the need for further research concerning the influence of external forcings versus internally generated climate variability by analysing ensembles of transient model runs together with different independent reconstruction approaches as a prerequisite for reliable assessments of future climate change.

References

Barnston AG, Lizevey RE (1987) Classification, seasonality, and persistence of low-frequency atmospheric circulation patterns. Mon Wea Rev 115:1083–1126

Baur F, Hess P, Nagel H (1944) Kalender der Grosswetterlagen Europas 1881–1939. Bad Homburg

Blunier T, Chappellaz J, Schwander J, Stauffer B, Raynaud D (1995) Variations in atmospheric methane concentration during the Holocene epoch. Nature 374:46–49

Cassou C, Terray L, Hurrell JW, Deser C (2004) North Atlantic winter climate regimes: spatial asymmetry, stationarity with time and oceanic forcing. J Climate 17:1055–1068

Charney JG, DeVore JG (1979) Multiple flow equilibria in the atmosphere and blocking. J Atmos Sci 36:1205–1216

Cook ER, Briffa KR, Jones PD (1994) Spatial regression methods in dendroclimatology – a review and comparison of two techniques. Int J Climatol 14:379–402

Corti S, Molteni F, Palmer TN (1999) Signature of recent climate change in frequencies of natural atmospheric circulation regimes. Nature 398:799–802

Crowley TJ (2000) Causes of climate change over the past 1000 years. Science 289:270–277

DeSwart HE (1988) Vacillation and predictability properties of low-order atmospheric spectral models. PhD thesis, Utrecht University, The Netherlands

Etheridge DM, Steele LP, Langenfelds RL, Francey RJ, Barnola JM, Morgan VI (1996) Natural and anthropogenic changes in atmospheric CO2 over the last 1000 years from air in Antarctic ice and firn. J Geophys Res 101:4115–4128

Exner FM (1924) Monatliche Luftdruck- und Temperaturanomalien auf der Erde. Sitzungsberichte d Kaiserl Akad der Wissenschaften 133:307–408

Glaser R, Brázdil R, Pfister C, Dobrovólny P, Barriendos Vallvé M, Bokwa A, Camuffo D, Kotyza O, Limanówka D, Rácz L, Rodrigo FS (1999) Seasonal temperature and precipitation fluctuations in selected parts of Europe during the sixteenth century. Clim Change 43:169–200

Handorf D, Petoukhov VK, Dethloff K, Eliseev AV, Weisheimer A, Mokhov II (1999) Decadal climate variability in a coupled atmosphere-ocean climate model of moderate complexity. J Geophys Res 104:27253–27276

Handorf D, Dorn W, Dethloff K, Rinke A, Weisheimer A (2004) Internal climate variability in global and regional climate models. In: Fischer H, Kumke T, Lohmann G, Flöser G, Miller H, von Storch H, Negendank JFW (eds) The KIHZ project: towards a synthesis of Holocene proxy data and climate models. Springer, Berlin Heidelberg New York, pp 365–382

Hannachi A (1997) Low-frequency variability in a GCM: three-dimensional flow regimes and their dynamics. J Climate 10:1357–1379

Hasselmann K (1999) Climate change–linear and nonlinear signatures. Nature 398:755–756

Hoerling MP, Hurrell JW, Xu T (2001) Tropical origins for recent North Atlantic climate change. Science 292:90–92

Hsu CJ, Zwiers F (2001) Climate change in recurrent regimes and modes of Northern Hemisphere atmospheric variability. J Geophys Res 106:20145–20159

Hurrell JW, van Loon H (1997) Decadal Variations associated with the North Atlantic Oscillation. Clim Change 36:301–326

Hurrell JW, Hoerling MP, Phillips AS, Xu T (2004) Twentieth century North Atlantic climate change. Part 1: assessing determinism. Clim Dyn. 23:371-389

Kalnay E et al. (1996) The NCEP/NCAR 40-Year Reanalysis Project. B Am Meteorol Soc 77:437–471

Kimoto M, Ghil M (1993a) Multiple flow regimes in the Northern Hemisphere winter. Part I: methodology and hemispheric regimes. J Atmos Sci 50:2625–2643

Kimoto M, Ghil M (1993b) Multiple flow regimes in the Northern Hemisphere winter. Part II: sectorial regimes and preferred transitions. J Atmos Sci 50:2645–2673

Kistler R et al. (2001) The NCEP-NCAR 50-year reanalysis: monthly means CD-ROM and documentation. B Am Meteorol Soc 82:247–267

Klein WH, Dai Y (1998) Reconstruction of monthly mean 700-mb heights from surface data by reverse specification. J Climate 11:2136–2146

Kosloswski G, Glaser R (1999) Variations in reconstructed ice winter severity in the Western Baltic from 1501–1995, and their implications for the North Atlantic Oscillation. Clim Change 41:175–191

Kumar P, Foufoula-Georgiou E (1997) Wavelet analysis for geophysical applications. Rev Geophys 35:385

Legras B, Ghil M (1985) Persistent anomalies, blocking, and variations in atmospheric predictability. J Atmos Sci 42:433–471

Legutke S, Voss R (1999) The Hamburg atmosphere-ocean coupled circulation model ECHO-G. DKRZ Tech Rep 18, DKRZ, Hamburg, Germany, pp 74

Lorenz EN (1963) Deterministic nonperiodic flow. J Atmos Sci 20:130–141

Luterbacher J, Rickli R, Xoplaki E, Tinguely C, Beck C, Pfister C, Wanner H (2001) The late maunder minimum (1675–1715) – a key period for studying decadal scale climatic change in Europe. Clim Change 49:441–462

Luterbacher J, Xoplaki E, Dietrich D, Rickli R, Jacobeit J, Beck C, Gyalistras D, Schmutz C, Wanner H (2002) Reconstruction of sea level pressure fields over the Eastern North Atlantic and Europe back to 1500. Clim Dyn 18:545–561

Mo K, Ghil M (1988) Cluster analysis of multiple planetary flow regimes. J Geophys Res 93:10927–10952

Molteni F, Sutera A, Tronci N (1988) The EOFs of the geopotential eddies at 500 mb in winter and their probability density function. J Atmos Sci 45:3063–3080

Monahan AH, Fyfe, JC, Flato, GM (2000) Northern Hemisphere atmospheric variability and change under global warming. Geophys Res Lett 27:1139–1142

Monahan AH, Pandolfo L, Fyfe JC (2001) The preferred structure of variability of the Northern Hemisphere atmospheric circulation. Geophys Res Lett 28:1019–1022

North G, Bell T, Cahalan R, Moeng F (1982) Sampling errors in the estimation of empirical orthogonal functions. Mon Wea Rev 110:699–706

Palmer TN (1993) Extended-range atmospheric prediction and the Lorenz model. B Am Meteorol Soc 74:49–65

Palmer TN (1999) A nonlinear dynamical perspective on climate prediction. J Climate 12:575–591

Pfister C (1999) Wetternachhersage. Haupt, Bern Stuttgart Wien

Raible CC, Luksch U, Fraedrich K, Voss R (2001) North Atlantic decadal regimes in a coupled GCM simulation. Clim Dyn 18:321–330

Roeckner E, Arpe K, Bengtsson L, Christoph M, Claussen M, Dümenil L, Esch M, Giorgetta M, Schlese U, Schulzweida U (1996) The atmospheric general circulation model ECHAM-4: Model description and simulation of present-day climate. MPI Rep 218, Max Planck Institute for Meteorology, Hamburg

Rossby CG (1939) Relation between variations in the intensity of the zonal circulation of the atmosphere and the displacements of the semi-permanent centers of action. J Mar Res 2:38–55

Silverman BW (1986) Density estimation for statistics and data analysis. Chapman and Hall, New York

Slonosky VC, Jones PD, Davies TD (2000) Variability of the surface atmospheric circulation over Europe, 1774–1995. Int J Climatol 20: 1875–1897

Stephenson DB, Hannachi A, O'Neill A (2004) On the existence of multiple climate regimes. Quat J Roy Meteor Soc 130:583–606

von Storch H, Zwiers FW (1999) Statistical analysis in climate research. Cambridge University Press, Cambridge

Torrence C, Compo GP (1998) A practical guide to wavelet analysis. B Am Meteorol Soc 79:61–78

Vautard R (1990) Multiple weather regimes over the North Atlantic: analysis of precursors and successors. Mon Wea Rev 118:2056–2081

Walker GT (1924) Correlation in seasonal variation of weather, IX. Mem Ind Met Dept 25:275–332

Wallace JM, Gutzler DS (1981) Teleconnections in the geopotential height field during Northern Hemisphere winter. Mon Wea Rev 109:784–812

Wanner H, Pfister C, Brázdil R, Frich P, Frydendahl K, Jónsson T, Kington J, Lamb HH, Rosenørn S, Wishman E (1995) Wintertime European circulation patterns during the Late Maunder Minimum cooling period (1675–1704). Theor Appl Climatol 58:159–165

Weisheimer A, Handorf D, Dethloff K (2001) On the structure and variability of atmospheric circulation regimes in coupled climate models. Atmos Sci Lett 2:72–80

Wolff JO, Maier-Reimer E, Legutke S (1997) The Hamburg ocean primitive equation model. DKRZ Tech Rep 13, DKRZ, Hamburg

Yang S, Reinhold B (1991) How does the low-frequency variance vary? Mon Wea Rev 119:119–127

Zorita E, González-Rouco JF (2002) Are temperature sensitive proxies adequate for North Atlantic Oscillation reconstructions? Geophys Res Lett 29, DOI 10.1029/2002GL015404

Zorita E, von Storch H, González-Rouco JF, Cubasch U, Luterbacher J, Legutke S, Fischer-Bruns I, Schlese U (2004) Climate evolution in the last five centuries simulated by an atmosphere-ocean model: global temperatures, the North Atlantic Oscillation and the Late Maunder Minimum. Meteor Z 13:271–289